Asian Journal of Chemistry; Vol. 32, No. 9 (2020), 2335-2341

ASIAN JOURNAL OF CHEMISTRY

https://doi.org/10.14233/ajchem.2020.22829

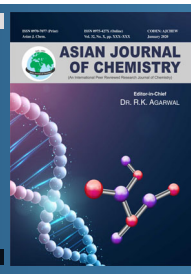

# Comparative Study of Structural, Morphological and Humidity Sensing Properties of Pure $WO_3$ and $Cu_2O$-$WO_3$ Nanocomposite

Narendra Kumar Pandey[1], Sanchita Singh[1,*] and Priya Gupta[2]

[1]Sensors and Materials Research Laboratory, Department of Physics, University of Lucknow, Lucknow-226007, India
[2]Electronics and Communication Engineering Department, Integral University, Lucknow-226026, India

*Corresponding author: E-mail: s.sanchita24@gmail.com

*Received*: 18 May 2020; *Accepted*: 24 June 2020; *Published online*: 20 August 2020; AJC-20035

This work reports the enhancement of humidity sensing properties of tungsten trioxide ($WO_3$) by the formation of nanocomposite with cuprous oxide ($Cu_2O$). A 0.1 g of $Cu_2O$ was mixed with 0.9 g of $WO_3$. Pellets of pure $WO_3$ and the obtained mixture are prepared at pressure of 250 MPa applied for 0.5 h. The pellets were then annealed at 300 ºC, 400 ºC, 500 ºC and 600 ºC. X-ray diffraction (XRD) and scanning electron microscopy (SEM) analyzed the crystallinity and morphology of as-prepared pellets surface. Humidity sensing application of pellets is studied in a specially designed chamber. It is observed that as relative humidity increases, there is decrease in the resistance of the pellets. The humidity-sensing investigation (10-99%RH) showed that the nanocomposite of $Cu_2O$ with $WO_3$ annealed at 600 ºC, is having the best sensitivity, low hysteresis, less ageing and high reproducibility than pure $WO_3$. It is also observed that as annealing temperature increases from 300 to 600 ºC, sensitivity increases. The present investigation could be useful for fabrication of resistive type humidity sensors for commercial applications.

**Keywords: Sensor, Humidity, Adsorption, Hysteresis, Porosity.**

## INTRODUCTION

Metal oxides/metal oxides composite have wide applications as catalyst [1], gas sensors [2], antifungal agents [3] adsorbents [4] and energy conversion [5]. There are various metal oxides like ZnO, $TiO_2$, CuO, NiO, *etc*. which have been used in the designing of different types of sensors. Tungsten trioxide ($WO_3$) is an n-type semiconductor having a band gap in the range 2.5-2.8 eV, received much interest in the applications like photocatalysis [6-9], electrochromic devices [10-12], solar energy conversion [13] and gas sensors [14], and many more due to its excellent catalytic, optical and dielectric properties, good physical and chemical stability.

Humidity sensors are of very high importance due to their increasing uses in various industries as well as in scientific laboratories. There are many domestic applications of humidity sensors such as in controlling cooking for microwave ovens, intelligent control in buildings and laundry, *etc*. In automobile industries, humidity sensors are used in rear window defoggers and motor assembly lines. In medical fields, humidity sensors are used in sterilizers, respiratory equipment, pharmaceutical processing, incubators and biological products. In agriculture, humidity sensors are used for green-house air-conditioning, plantation protection (dew prevention), soil moisture monitoring, and cereal storage. In general industry, humidity sensors are used for humidity control in chemical gas purification, dryers, ovens, film desiccation, paper and textile production and food processing [15]. Humidity sensors that are developed using metal oxides have attracted much attention due to their chemical and physical stability. Metal oxides having larger surface area and smaller grain size finds remarkable applications in humidity sensing. Upon exposure to the moisture on sample surface, the water molecules get dissociated and are adsorbed at these defect sites. This leads to an enhancement in the surface electron concentration [16]. Various humidity sensors have also been developed using metal oxides that provide high sensitivity, linear response, low response time and low power consumption. Leng *et al.* [17] prepared $WO_3$ nanofibers using an electrospinning method of fabrication. Teoh *et al*. [18] reported that $WO_3$ thin film having mesoporous morphology exhibits pores

with an average size of 5 nm and its specific surface area of 151 $m^2/g$. Yan *et al*. [19] synthesized $WO_3$ nanowall using solvothermal, whereas Shakya *et al*. [20] reports the humidity sensing properties of ZnO-$WO_3$ nanocomposite and found that 5% ZnO doped $WO_3$ showed highest sensitivity of 20.95 MΩ/%RH in 15-95%RH range. Liu *et al*. [21] have synthesized tungsten oxide nanorods assembled microspheres by a facile hydrothermal process. Zhou *et al*. [22] have synthesized the highly ordered mesoporous tungsten oxides *via* hard templating method using mesoporous silica as a hard template and phosphotungstic acid as a precursor. Misra *et al*. [23] reported humidity sensing properties of pure and $Al_2O_3$ doped ZnO samples in the form of pellets prepared through solid state route reactions. It is observed that the resistance of pellets decreased for the range of humidity from 10%RH to 90%RH. Sample doped with 15 wt% of $Al_2O_3$ in ZnO and annealed at 700 ºC shows the best results with sensitivity of 14.98 M/%RH. It is also observed that for this sensing element repeatability over different cyclic operations is within ± 2% after 6 months and its response and recovery times are found to be 85 and 286 s, respectively [23]. Kumar *et al*. [24] prepared polyaniline (PANI) thin films by spin coating and when exposed to humidity, it shows good response to humidity leading to development of commercial humidity sensor using polymers in future. Khadse *et al*. [25] fabricated a highly sensitive and fast humidity sensor based on cerium oxide nanoparticles, which are prepared at low cost *via* a simple non-isothermal precipitation method. $CeO_2$ nanoparticles based humidity sensors exhibit high and linear response within the whole relative humidity (RH) range of 11-97% at an operating frequency of 60 Hz. The corresponding impedance changes by approximately three orders of magnitude within the entire humidity range from 11% to 97% RH. The response and recovery times for this sample are about 2-3 and 9-10 s, respectively, when RH was switched between 11% and 97%. Furthermore, the sensors also show relatively small hysteresis, excellent reproducibility, long term stability and broad range of operation (11-97% RH) [25].

Several attempts have been made by the researchers to enhance the sensitivity of metal oxide based humidity sensors. One of which includes doping with other metal oxide/metal which is an effective method for improving its sensitivity. In this work, we have reported the characterization of the prepared samples using X-ray diffraction (XRD) and scanning electron microscopy (SEM) and humidity sensing properties of pure WO and $Cu_2O$-WO nanocomposites prepared by solid state reaction route are studied at various annealing temperatures. The humidity sensing performance of $Cu_2O$-$WO_3$ nanocomposite is also evaluated by measuring essential sensing parameters such as ageing effect, hysteresis, reversibility and stability in the 10-99%RH range.

## EXPERIMENTAL

Tungsten trioxide ($WO_3$) powder (Loba Chemie, 99.99%) and cuprous oxide ($Cu_2O$) powder were used as a main material for the preparation of samples. All pellet samples were prepared using solid state reaction route. For the preparation of pure $WO_3$ pellet, 1 g of pure $WO_3$ powder is added with 5 wt% polyvinyl alcohol (PVA) with acts as a binder to increase the strength of pellet. The obtained mixture is grinded uniformly in mortar and pestle for 3 h. The resultant powder is then pressed into pellet shape by applying uniaxial pressure of 250 MPa in a hydraulic press machine (M.B. Instruments, Delhi, India) at room temperature. The prepared pellets were in disc shape having diameter of 12 mm and thickness 2 mm. Nanocomposite of $Cu_2O$-$WO_3$ was also prepared by the similar procedure. The only difference was the addition of 0.1 g of $Cu_2O$ in 0.9 g of $WO_3$. The pellet samples are then annealed at temperatures of 300 ºC, 400 ºC, 500 ºC and 600 ºC for 3 h in an electric muffle furnace.

**Humidity sensing setup:** The samples were exposed to humidity (10-99%RH) in a specially designed humidity control chamber as shown in Fig. 1. Inside the humidity chamber, a thermometer (± 1 ºC) and standard hygrometer (digital, ±1% RH) were placed for the purpose of calibration. Variation in a resistance is recorded by a multifunctional digital multimeter (±0.001 MΩ.VC-9808) with respect to change in percentage relative humidity. The potassium sulphate solution was used as a humidifier, while KOH solution was used as a dehumidifier. For measuring the resistance of pellets, copper electrodes were used. Two thin copper plates were used for making the electrical contacts on the surfaces of pellets. The copper sheets were put in such a way to cover the two opposite cross sectional areas of pellet. In order to see the effect of ageing, humidity sensing property of these elements was examined again after six months in same humidity control chamber under the same conditions.

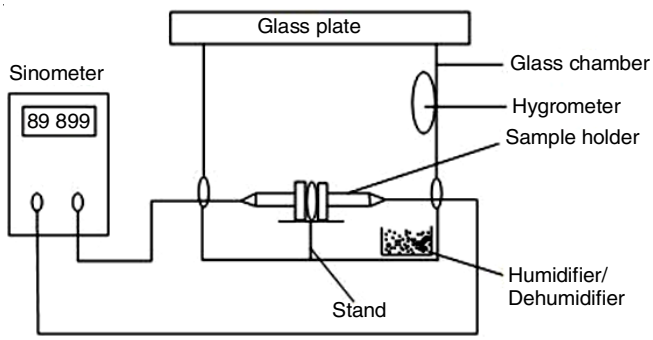


Fig. 1. Set up of humidity control chamber

## RESULTS AND DISCUSSION

**SEM analysis:** Surface morphology of pellet samples was studied using scanning electron microscope (SEM, LEO-0430, and Cambridge). Fig. 2a-b show the micrographs of pure $WO_3$ and $Cu_2O$-$WO_3$ nanocomposite, respectively annealed at 600 ºC. SEM images showed that the morphology of nanoparticles was spherical with some elongation and having highly porous structure. These pores were expected to provide sites for humidity adsorption therefore, increases the humidity sensitivity of material. The grain size of pure $WO_3$ was 158 nm and $Cu_2O$-$WO_3$ nanocomposite was found to be 159 nm. Highly porous structure of $Cu_2O$-$WO_3$ nanocomposite offers more sites for interaction of water molecules offering maximum sensitivity. Higher porosity increases the surface to volume ratio of the material and enhances the diffusion rate of water into or out of porous structure and thus helps in getting good sensitivity.

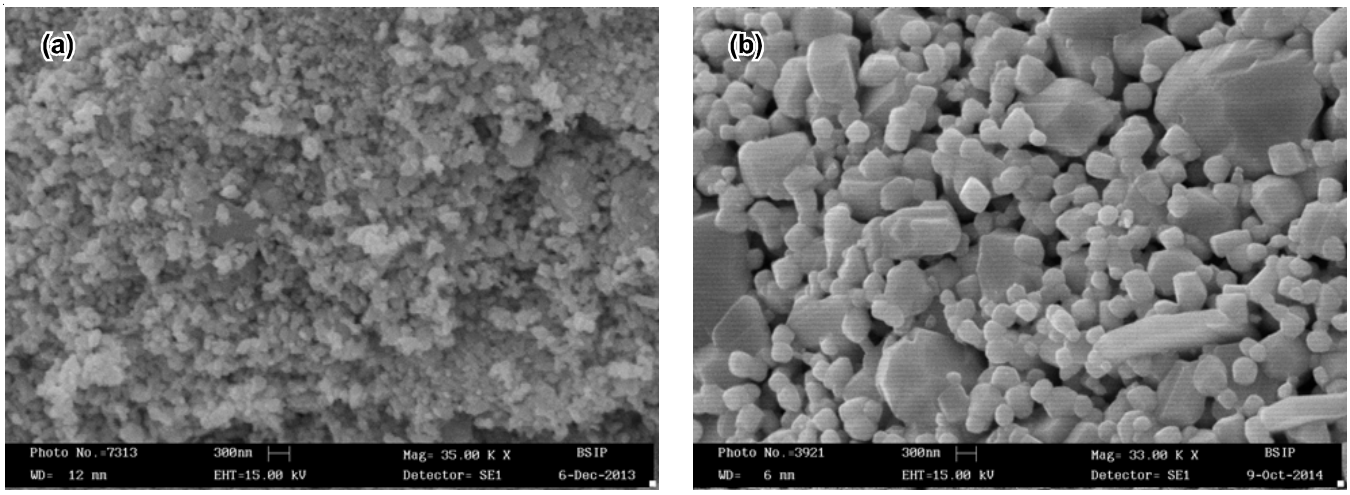


Fig. 2. SEM images of (a) pure $WO_3$ (WC-0) and (b) $Cu_2O$-$WO_3$ (WC-10) nanocomposite annealed at 600 °C

**Powder XRD analysis:** X-ray diffraction was studied using X-pert PRO Analytical XRD system (Netherland) having Cu*K*α radiation source of wavelength 1.5406 Å. Fig. 3a-b shows X-ray diffraction pattern for pure $WO_3$ and $Cu_2O$-$WO_3$ nanocomposite at annealing temperature 600 ºC. The average crystallite size of the samples was calculated using Debye Scherer′s formula:

$$D = \frac{K\lambda}{\beta\cos\theta} \quad (1)$$

where D is the crystallite size, K is the fixed number of 0.9, λ is the X-ray wavelength, θ is the Bragg′s angle (radian) and β is the full width at half maximum of the peak (radian). The crystallite size calculated from the Scherer′s formula for pure $WO_3$ sample was 72.4 nm, while for $Cu_2O$-$WO_3$ nanocomposite was 74.4 nm.

The main characteristic diffraction peaks at 600 ºC correspond to the (001), (110), (101), (111), (200), (201), (102), (221), (310), (212), (400), (401), (331), (203) and (421) planes at 2θ equal to 21.8º, 24.3º, 28.6º, 32.7º, 34.1º, 41.8º, 49.9º, 54.3º, 55.9º, 62.2º, 71.9º, 76.9º, 81.6º, 83.3º and 86.1º, respectively for pure $WO_3$. The diffraction peaks of $Cu_2O$ [(111) and (200)] at 44.3º and 50.4º can be observed obviously. These peaks were well matched with the diffraction lines reported in JCPDS card no. 00-005-0388 for tungsten oxide and JCPDS card no. 01-071-3645 for cuprous oxide.

Majority of peaks [(101), (111), (201), (221), (401)] were shifted towards slightly lower value of diffraction angle while some shifted at higher value [(001), (110), (200), (212)] and some maintained their previous value [(102), (310), (400)]. Appearance of few $Cu_2O$ peaks in XRD indicated the atomic substitution of $Cu_2O$ in $WO_3$ rather than interstitial substitution. Majority of the diffraction peaks shifted slightly towards lower 2θ angles for $Cu^+$ doping, which is due to the occupancy of $W^{6+}$ (0.78 Å) sites by $Cu^+$ (0.77 Å) (Fig. 3) causing some kind of lattice distortion that is induced by the stress during the preparation [26]. The crystallite size increased in the case of $Cu_2O$-$WO_3$ nanocomposite annealed at 600 ºC as compared to pure $WO_3$. This increase in crystallite size might be due to the lattice strain induced in the $Cu_2O$-$WO_3$ nanocomposite caused by the small mismatch of ionic radii between the $W^{6+}$ and $Cu^+$. The shifting of XRD peaks and a corresponding increase in crystallite size suggest that $Cu^+$ ions were successfully incorporated into the $WO_3$ without altering the overall crystal structure.

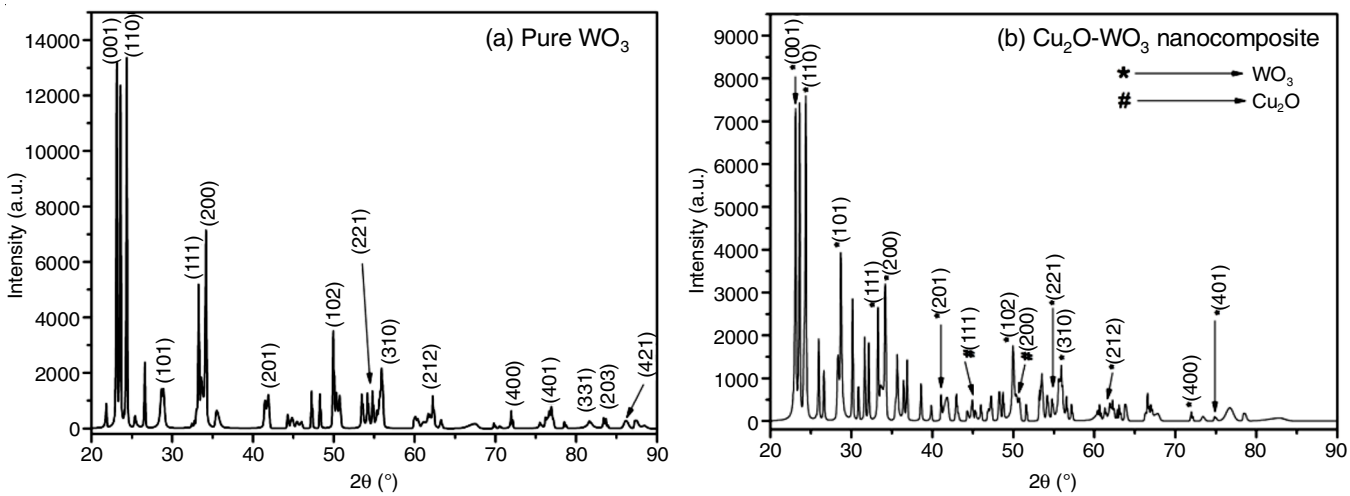


Fig. 3. XRD patterns of (a) (WC-0) and (b) (WC-10) nanocomposite annealed at 600 ºC

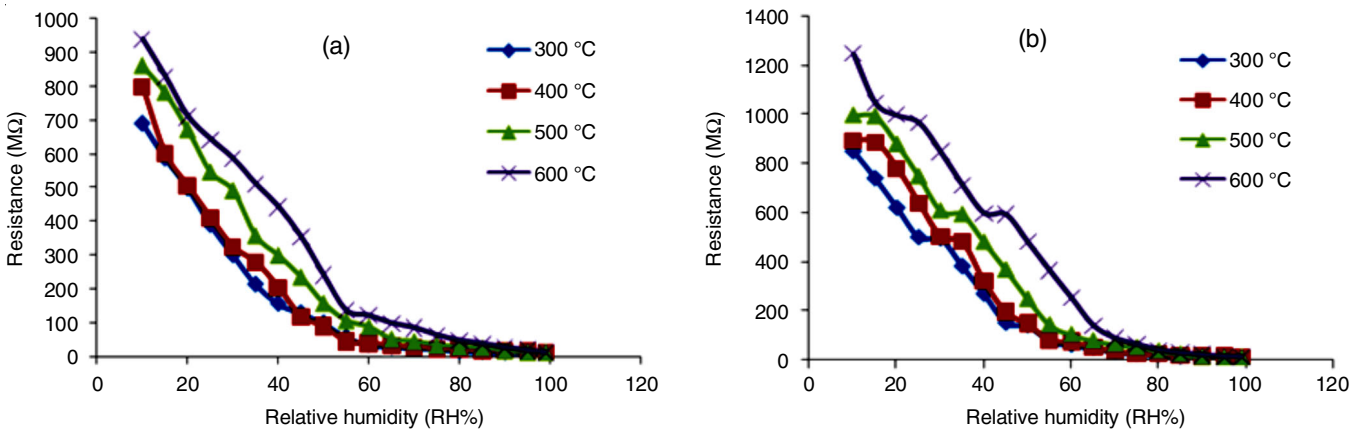


Fig. 4. Humidification graphs for (a) pure $WO_3$ and (b) $Cu_2O$-WO nanocomposites annealed at temperature 300°C to 600 °C

**Humidification graph:** The variation in sensor resistance with different percentage relative humidity values (10-99%RH) for pure $WO_3$ and $Cu_2O$-$WO_3$ nanocomposite is shown in Fig. 4. It is clearly seen that addition of $Cu_2O$ in $WO_3$ increases the electrical conductivity of the pellet sample. It wass noticed that with an increase in the %RH level, the obtained resistance of sensor shifted to the lower values monotonically. The adsorbed water molecules lower the resistance by 2-D capillary effect and can strengthen the space-charge polarization effect and initiate fast diffusion into the inner portion of $Cu_2O$-$WO_3$ nanocomposite pellet [27]. Additionally, this will also help the formation of protons between the hydroxyl-containing groups. Among all the samples, $Cu_2O$-$WO_3$ nanocomposite sample annealed at 600 ºC exhibited the highest sensitivity. Sensitivity of the humidity sensor is defined as the change in resistance (ΔR) of the sensing element per unit change in relative humidity (%RH). The sensitivity of the sample is calculated by using the following formula:

$$S = \frac{\Delta R}{\Delta RH\%} \quad (2)$$

where ΔR is the change in resistance and ΔRH% is the change in percentage relative humidity.

When the relative humidity increases from 10%RH to 99%RH, for pure $WO_3$ the sensitivity increases from 7.64 MΩ/%RH to 10.40 MΩ/%RH with increase in annealing temperature from 300 ºC to 600 ºC as shown in Fig. 5. An increase in sensitivity value with temperature was mainly attributed to nanopores, which facilitate high surface area for water molecules to diffuse across the sample. While for $Cu_2O$-$WO_3$ nanocomposite, sensitivity increases from 9.44 MΩ/%RH to 13.88 MΩ/%RH. The sensitivity for pure $WO_3$ sample was significantly lower than the sensitivity obtained for $Cu_2O$-$WO_3$ nanocomposite under the same conditions. The increment in the sensing capability of $Cu_2O$-$WO_3$ nanocomposite was due to the presence of water molecules in the extended interlayer, which increases charge storage capability [28]. With increase in %RH, the succeeding water molecules attached with the first water layer and result in a continuous water adsorption by layer-by-layer permeation. This was possible because of the attachment of water molecule with the H-bond through hydroxyl groups. At high

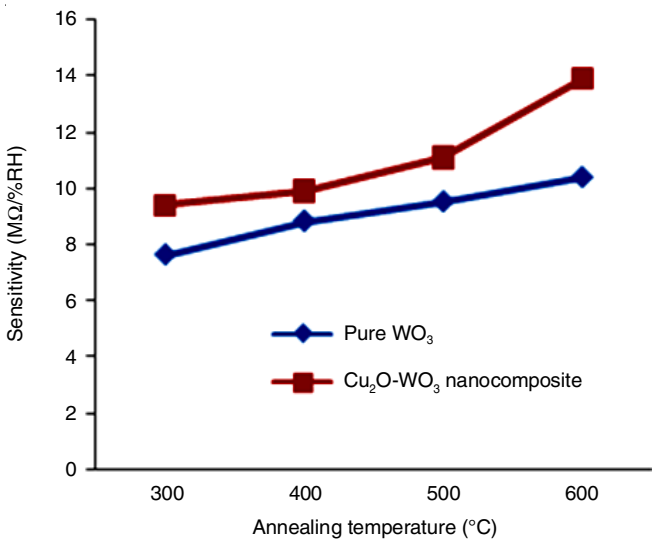


Fig. 5. Characteristics of sensitivity with annealing temperature 300 to 600 °C for pure $WO_3$ and $Cu_2O$-WO nanocomposites

relative humidity (> 50%RH), liquid water condensed in the capillary like pores, forming a liquid like layer. A decrease in the value of resistance or increase of conductance might also occur due to variation of grain boundary barrier height in metal oxides. In this case, adsorption of water molecules at metal oxide surface penetrated inside the sample can decrease the height of potential barriers at the surface grains and at the surface of necks between metal oxide grains. Therefore, size of depletion regions in the vicinity of necks in the direction of electric field was lowered and conductance of ceramics increased. Penetrated water molecules could promote decrease in barrier height of grain boundary potential exponentially and even slight decrease of grain boundary barrier height due to relative humidity can cause substantial decrease of resistance (or increase of conductance).

**Hysteresis:** Hysteresis in metal oxides occurs mainly due to the chemisorption and physisorption processes. The hysteresis is mainly attributed to the initial chemisorptions on the surface of the samples. This chemisorbed layer is not easily affected by exposure to atmosphere but can only be desorbed thermally. On the other side, the physisorbed layer can be easily desorbed.

Hence, in the dehumidification process, initially adsorbed water was not removed completely leading to hysteresis. The hysteresis deteriorates the efficiency of sensor by increasing the time lag in the continuous process of adsorption and desorption. In this work, the hysteresis error (γH) was calculated using the expression [29]:

$$\gamma H = \pm \frac{\Delta H_{max}}{2F_{FS}} \quad (3)$$

where, $\Delta H_{max}$ is the difference in output of adsorption and desorption processes and FFS is the full scale output. To determine the hysteresis effect in the sensing elements, the humidity in the chamber had been increased from 10% RH to 99% RH and the values of resistance of the samples recorded with change in %RH. All sensing elements show acceptable hysteresis values. The value of hysteresis for pure $WO_3$ and $Cu_2O$-$WO_3$ nanocomposite were 0.47% and 0.18%, respectively at 600 ºC annealed temperature. It was observed that hysteresis decreases in case of composite as compared to pure $WO_3$. Fig. 6a-b shows the hysteresis graphs for pure $WO_3$ and $Cu_2O$-$WO_3$ nanocomposite respectively, annealed at 600 ºC.

**Ageing effect:** Ageing is one of the major drawbacks of metal oxides based humidity sensors. For analyzing the effect of ageing, the sensing properties of pure $WO_3$ and $Cu_2O$-$WO_3$ nanocomposite annealed at 600 ºC was examined again in the humidity control chamber under the same conditions after six months. The variation of resistance of both pure and nanocomposite sensing elements with change in %RH after six months is shown in Fig. 7a-b. It was observed that average sensitivity in the range 10%RH to 99%RH for pure $WO_3$ annealed at 600 ºC was 10.40 MΩ%RH and after six months decreases to 8.87 MΩ%RH is shown in Table-1. The value of average sensitivity for $Cu_2O$-$WO_3$ nanocomposite annealed at 600 ºC was 13.88 MΩ%RH and after six months it decreases to 11.44 MΩ%RH. The values have been found to be stable within +5% of measured values after six months. In humidity sensors ageing mechanism may be due either to prolonged exposure of surface to high humidity, adsorption of contaminants preferentially on the cation sites, loss of surface cations due to vaporization, solubility and diffusion or annealing to a less reactive structure, migration of cations away from the surface due to thermal diffusion.

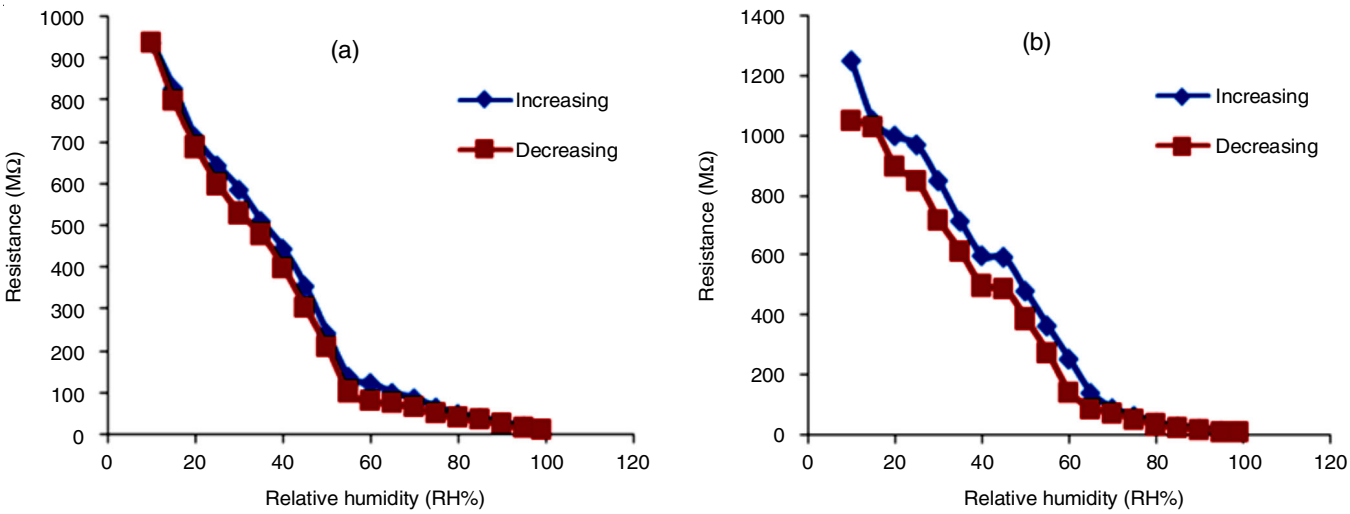


Fig. 6. Hysteresis graph for (a) pure $WO_3$ and (b) $Cu_2O$-WO nanocomposites at annealing temperature 600 °C

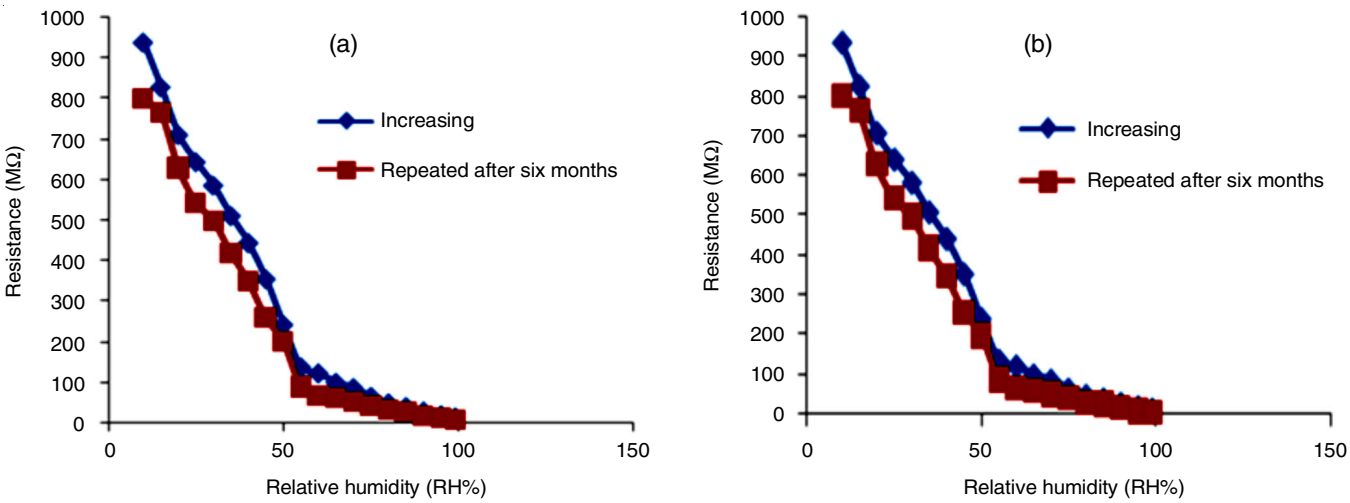


Fig. 7. Variation of resistance for (a) pure $WO_3$ and (b) $Cu_2O$-WO nanocomposite annealed at 600 °C [after six months]

TABLE-1
SENSITIVITY OF PURE $WO_3$ AND $Cu_2O$-$WO_3$ NANOCOMPOSITES

| Annealing temperature (°C) | Sensitivity (MΩ%RH) | | | |
|---|---|---|---|---|
| | Pure $WO_3$ | $Cu_2O$-$WO_3$ nanocomposites | Pure $WO_3$ (after six months) | $Cu_2O$-$WO_3$ nanocomposites (after six months) |
| 300 | 7.64 | 9.44 | 6.85 | 8.86 |
| 400 | 8.84 | 9.92 | 7.75 | 9.89 |
| 500 | 9.53 | 11.10 | 9.98 | 10.53 |
| 600 | 10.40 | 13.88 | 8.87 | 11.44 |

**Sensing mechanism:** The nanocomposite based humidity sensors presented in the work are based on the interaction of water vapour with porous metal oxide surfaces, which results in change in electrical resistance of the pellet sample. The process of humidity sensing is generally occurs in two steps process: (i) **chemisorption:** at low percentage relative humidity, the water molecules are chemically bonded on sensor surface by means of hydrogen interactions and (ii) **physisorption:** at high percentage relative humidity, the successive layers of water molecules are condensed on the sensor surface to form water layers (Fig. 8). Only small amount of water molecules get adsorbed on the surface of dry sensor under the low relative humidity conditions, which results in the formation of the first chemisorption layer through double hydrogen bonding with the W-OH groups. This small amount of water molecules forms a discontinuous layer, which disrupts the smooth propagation of charge carriers across the sensor surface. Only few water molecules were chemisorbed at this time to form hydroxyl groups on the activated sites of grain surface of sensor and protons may be transferred from surface hydroxyl (W-OH) groups to water molecules to form $H_3O^+$ as shown by eqn. 4:

$$2H_2O \rightarrow H_3O^+ + OH^- \quad (4)$$

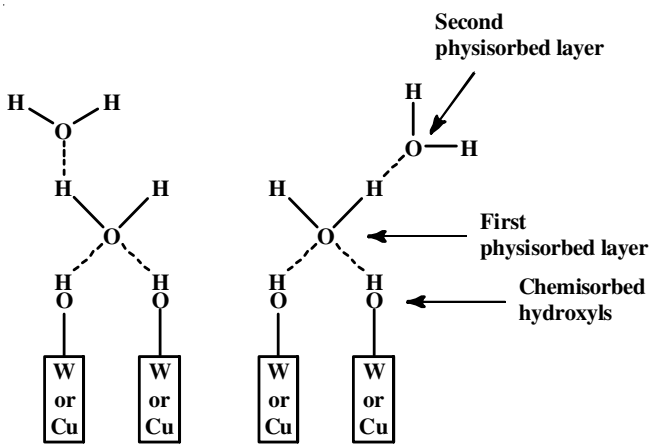


Fig. 8. Sensing mechanism of solid state humidity sensor

The chemisorbed layer, once formed, was not further affected by exposure to humidity, however, with the increase in relative humidity (50%), the water molecules get physically adsorbed on the surface hydroxyl group layer to form physically adsorbed water layers. At this stage, the conduction occurs through the proton "hopping" between adsorption sites as per the Grothuss chain mechanism (eqn. 5):

$$H_2O + H_3O^+ \rightarrow H_3O^+ + H_2O \quad (5)$$

This inturn promotes the energetic hydration of $H_3O^+$ in liquid water as $H_3O^+ \rightarrow H_2O + H^+$, which facilitates the transportation of proton thereby leading to increase in conductivity of the sensor. At the 99%RH conditions, more layers of water molecules gets physically adsorbed on the prior adsorbed water molecules and resemble to bulk water. At this time, $H^+$ ions travel freely on the surface of sensor and as a resultant a significant decrease in impedance of the sensor was observed [30].

## Conclusion

In this work, pure $WO_3$ and $Cu_2O$-$WO_3$ nanocomposites were prepared by using solid state reaction. The crystallite size increased to 74.4 nm from 72.4 nm when pure $WO_3$ form nanocomposite with $Cu_2O$ for annealing temperature at 600 ºC. It was observed that an insignificant $Cu_2O$ peaks appeared in XRD pattern which indicate atomic substitution of $Cu_2O$ atoms rather than interstitial substitution. SEM images revealed that the samples having spherical morphology with pores on the surface and its grain size were increased from 158 nm to 159 nm with addition of $Cu_2O$ atoms in pure $WO_3$. The larger grain size indicated agglomeration of crystallites near interstitials. When pellet samples are exposed to humidity, its sensitivity increased with an increase in annealing temperature for both pure and nanocomposite sample. The $Cu_2O$-$WO_3$ nanocomposite sample annealed at 600 ºC showed best sensitivity of 13.88 MΩ/%RH. The problem of hysteresis and ageing was also reduced in case of nanocomposite. As $Cu_2O$-$WO_3$ nanocomposite shows an improved sensitivity with low hysteresis and high reproducibility, it proved to be a robust, low cost, high strength sensor for humidity sensing.

## CONFLICT OF INTEREST

The authors declare that there is no conflict of interests regarding the publication of this article.

## REFERENCES

1. L. Andronic, L. Isac and A. Duta, *J. Photochem. Photobiol. Chem.*, **221**, 30 (2011); https://doi.org/10.1016/j.jphotochem.2011.04.018
2. A. Dey, *Mater. Sci. Eng. B*, **229**, 206 (2018); https://doi.org/10.1016/j.mseb.2017.12.036
3. J. Sawai and T. Yoshikawa, *J. Appl. Microbiol.*, **96**, 803 (2004); https://doi.org/10.1111/j.1365-2672.2004.02234.x
4. R. Taman, M.E. Ossman, M.S. Mansour and H.A. Farag, *J. Adv. Chem. Eng.*, **5**, 125 (2015); https://doi.org/10.4172/2090-4568.1000125
5. G. Wang, Y. Yang and D. Han and Y. Li, *NanoToday*, **13**, 23 (2017); https://doi.org/10.1016/j.nantod.2017.02.009
6. P.-G. Su, *Talanta*, **59**, 667 (2003); https://doi.org/10.1016/S0039-9140(02)00582-9

7. I. Aslam, M.H. Farooq, M.W. Iqbal, R. Boddula, M. Abid, M. Ashfaq and U. Ghani, *Mater. Sci. Ener. Technol*., **2**, 187 (2019); https://doi.org/10.1016/j.mset.2019.02.002
8. C.-M. Wu, S. Naseem, M.H. Chou, J.H. Wang and Y.Q. Jian, *Front. Mater*., **6**, 49 (2019); https://doi.org/10.3389/fmats.2019.00049
9. M. Sun, N. Xu, Y.W. Cao, J.N. Yao and E.G. Wang, *J. Mater. Res.*, **15**, 927 (2000); https://doi.org/10.1557/JMR.2000.0132
10. B.P. Jelle and G. Hagen, *Sol. Energy Mater. Sol. Cells*, **58**, 277 (1999); https://doi.org/10.1016/S0927-0248(99)00009-4
11. C.G. Granqvist, *Sol. Energy Mater. Sol. Cells*, **60**, 201 (2000); https://doi.org/10.1016/S0927-0248(99)00088-4
12. E. Llobet, G. Molas, P. Molinàs, J. Calderer, X. Vilanova, J. Brezmes, J.E. Sueiras and X. Correig, *J. Electrochem. Soc.*, **147**, 776 (2000); https://doi.org/10.1149/1.1393270
13. C.S. Rout, A. Govindraj and C.N.R. Rao, *J. Mater. Chem.*, **16**, 3936 (2006); https://doi.org/10.1039/B607012B
14. S. Luo, G. Fu, H. Chen and Y. Zhang, *Mater. Chem. Phys.*, **109**, 541 (2008); https://doi.org/10.1016/j.matchemphys.2008.01.015
15. Z. Chen and C. Lu, *Sens. Lett.*, **3**, 274 (2005); https://doi.org/10.1166/sl.2005.045
16. Q. Kuang, C. Lao, Z.L. Wang, Z. Xie and L. Zheng, *J. Am. Chem. Soc.*, **129**, 6070 (2007); https://doi.org/10.1021/ja070788m
17. J. Leng, X. Xu, N. Lv, H. Fan and T. Zhang, *J. Colloid Interface Sci.*, **356**, 54 (2011); https://doi.org/10.1016/j.jcis.2010.11.079
18. L.G. Teoh, I.M. Hung, J. Shieh, W.H. Lai and M.H. Hon, *Electrochem. Solid-State Lett.*, **6**, G108 (2003); https://doi.org/10.1149/1.1585252
19. A. Yan, C. Xie, D. Zeng, S. Cai and H. Li, *J. Alloys Compd.*, **495**, 88 (2010); https://doi.org/10.1016/j.jallcom.2010.01.092
20. V. Shakya, N.K. Pandey, S.K. Misra and A. Roy, *Bull. Mater. Sci.*, **40**, 253 (2017); https://doi.org/10.1007/s12034-017-1373-5
21. Z. Liu, M. Miyauchi, T. Yamazaki and Y. Shen, *Sens. Actuators B Chem.*, **140**, 514 (2009); https://doi.org/10.1016/j.snb.2009.04.059
22. L. Zhou, Q. Ren, X. Zhou, J. Tang, Z. Chen and C. Yu, *Micropor, Mesopor, Mater.*, **109**, 248 (2008); https://doi.org/10.1016/j.micromeso.2007.04.054
23. S.K. Misra, N.K. Pandey, V. Shakya and A. Roy, *IEEE Sens. J.*, **15**, 3582 (2015); https://doi.org/10.1109/JSEN.2015.2394321
24. R. Kumar and B.C. Yadav, *Mater. Lett.*, **167**, 300 (2016); https://doi.org/10.1016/j.matlet.2016.01.082
25. V.R. Khadse, S. Thakur, K.R. Patil and P. Patil, *Sens. Actuators B Chem.*, **203**, 229 (2014); https://doi.org/10.1016/j.snb.2014.06.107
26. K. Jonscher, Dielectric Relaxation in Solids, Chelsea Dielectric Press: London (1983).
27. H.-W. Yu, H.K. Kim, T. Kim, K.M. Bae, S.M. Seo, J.-M. Kim, T.J. Kang and Y.H. Kim, *ACS Appl. Mater. Interfaces*, **6**, 8320 (2014); https://doi.org/10.1021/am501151v
28. H. Bi, K. Yin, X. Xie, J. Ji, S. Wan, L. Sun, M. Terrones and M.S. Dresselhaus, *Sci. Rep.*, **3**, 2714 (2013); https://doi.org/10.1038/srep02714
29. R. Malik, V.K. Tomer, S. Duhan, S.P. Nehra and P.S. Rana, *Energy Environ. Focus*, **4**, 340 (2015); https://doi.org/10.1166/eef.2015.1182
30. A. Vijayan, M. Fuke, R. Hawaldar, M. Kulkarni, D. Amalnerkar and R.C. Aiyer, *Sens. Actuators B Chem.*, **129**, 106 (2008); https://doi.org/10.1016/j.snb.2007.07.113